Received: 9 May 2022 | Revised: 19 September 2022 | Accepted: 27 September 2022

DOI: 10.1111/ter.12625

RESEARCH ARTICLE

Terra Nova WILEY

Vertical deformation partitioning across a collapsing large and hot orogen

F. A. Temporim[1,2] | Ricardo Ivan Ferreirae da Trindade[1] | Marcos Egydio-Silva[3] | Tiago Valim Angelo[3] | Eric Tohver[1] | Caroline Cibele Soares[4] | Lucas Pequeno Gouvêa[5] | Julio Cesar Mendes[5] | Silvia Regina Medeiros[5] | Antônio Carlos Pedrosa-Soares[6] | Gabriel Gomes Silva[4]

[1]Instituto de Astronomia, Geofísica e Ciências Atmosféricas, Universidade de São Paulo, São Paulo, Brazil

[2]Faculdade de Ciências e Tecnologias, Universidade Federal de Goiás, Goiânia, Brazil

[3]Instituto de Geociências, Universidade de São Paulo, São Paulo, Brazil

[4]Centro de Ciências Exatas, Naturais e da Saúde, Universidade Federal do Espírito Santo, Alegre, Brazil

[5]Instituto de Geociências, Universidade Federal do Rio de Janeiro, Rio de Janeiro, Brazil

[6]Instituto de Geociências, Universidade Federal de Minas Gerais, Belo Horizonte, Brazil

Correspondence
F. A. Temporim, Instituto de Astronomia, Geofísica e Ciências Atmosféricas, Universidade de São Paulo, São Paulo, Brazil.
Email: filipetemporim@gmail.com

Funding information
Conselho Nacional de Desenvolvimento Científico e Tecnológico, Grant/Award Number: #405954/2016-6 and #304214/2018-3; Coordenação de Aperfeiçoamento de Pessoal de Nível Superior, Grant/Award Number: CAPES/SIU 0013; São Paulo Research Foundation, Grant/Award Number: #2016/06114-6 and #2017/11672-0

Abstract

Featuring 3000-km-long large and hot orogen, the Mantiqueira Province provides a rare opportunity to study the process of gravitational collapse at mid to deep crustal levels. Distinct but contemporary (~500 Ma) post-collisional intrusions show structures and anisotropy of magnetic susceptibility (AMS) fabrics related to their emplacements, recording different flow patterns. In southern deep-seated intrusions, ellipsoidal-shaped roots with gabbroic-to-hybrid cores surrounded by granitic rocks show concentric patterns of AMS fabrics that cut across the NE-trending regional foliation. In contrast, northern intrusions, exposed as the upper sections of batholith-size bodies of coarse-grained granite emplaced at the shallow to mid-crust, show general NS-trending magnetic fabrics roughly parallel to strike of the orogen and the regional foliation of host rocks. These contrasting magnetic patterns from shallow to deeper crust suggest vertical magma migration from the overthickened orogenic core to be emplaced across its thinner stretched flanks during the gravitational collapse of the orogenic edifice.

1 | INTRODUCTION

Large and hot orogens are characterized by wide plateaus developed over an overthickened crust, with high thermal gradients that cause partial melting on rocks in the middle and lower crust of the orogen's core (Vanderhaeghe & Teyssier, 2001a, 2001b). Crustal high heat production through radiogenic decay also tends to weaken the orogen's infrastructure (Henk et al., 2000). In the final stages, orogenic topography is flattened by erosion and gravitational collapse, whereby extension and crustal thinning reduce lateral gradients of gravitational potential energy through lateral flow of the hot orogenic interior towards its flanks (Rey et al., 2001). The geological expressions of these tectonic processes in a hot orogenic core are hard to decode since they usually overprint complex pre-collisional and syn-collisional structures.

The Mantiqueira Province (Figure 1) comprises several attributes expected for a large and hot orogen (Cavalcante et al., 2018; Caxito et al., 2022). The Araçuaí–Ribeira orogenic system (AROS) experienced intense magmatic activity between 630 and 480 Ma (Figure 1d) with a high-temperature regime sustained for ~90 m.y. in the orogen core, followed by a significant low in magmatic–metamorphic activity (ca. 540–520 Ma) before post-collisional igneous episodes (Araujo et al., 2020; Pedrosa-Soares et al., 2020). The syn-kinematic high-temperature regime assisted the development of a complex 3D deformation pattern (Alkmim et al., 2006), including orogen-parallel mass transport and stretching in the centre of the orogen (Cavalcante et al., 2018), building up the orogenic framework that came to host the post-collisional magmatism.

The post-collisional magmatism resulted in a series of intrusions which current exposed sections decrease in size from north to south along eastern AROS (defined in Figure 1c). They form composite stocks to batholiths, rich in magma mingling-mixing features of high-K calc-alkaline-ferroan A- and I-type granitic, and charnockitic rocks (De Campos et al., 2016; Serrano et al., 2018). Post-collisional intrusions found in the north have provided crystallization pressures around 2.4–3.5 kbar, while in the south they were emplaced at pressures around 5.7–11.5 kbar. The current exposure level represents a crustal section from former depths of ~10 km, in the north to ~35 km, in the south. In the north, post-collisional plutons form large, elongated, N-striking bodies parallel to the orogen. In contrast, in the south, the deep-seated sections of post-collisional intrusions consist mostly of round-shaped plutons with hybrid cores.

We performed a detailed mapping of magnetic fabrics using the anisotropy of magnetic susceptibility (AMS) of coeval plutons at different sectors of the belt, corresponding to different crustal levels. The presence of melt in a layer crustal section separated by fundamental rheological discontinuities and the lateral temperature gradients across the orogen implies that the strain may be heterogeneous on various scales. The internal fabric of granitic plutons results from the interplay between body forces due to magma chamber dynamics and the regional and gravitational stresses imposed onto the magma bodies. The vertical deformation partitioning across a collapsing large and hot orogen is much discussed by numerical models, but still little in natural cases.

2 | GEOLOGICAL SETTING

The AROS is an orogenic system about 2000 km long and 500 km wide (Figure 1). The N-trending Araçuaí orogen shows a double-verging hot core, comprising different assemblages of orogenic igneous rocks formed in distinct tectonic stages: the pre-collisional (630–580 Ma), syn-collisional (585–545 Ma), late-collisional (545–530 Ma) and post-collisional (530–480 Ma; Table S1). The main structural characteristic of pre-collisional magmatism is the N-striking regional foliation, often mylonitic, and structures imprinted by syn-collisional deformation. Similar to the pre-collisional, syn-collisional magmatism generally display the regional solid-state foliation.

Significance Statement

The manuscript presents a detailed mapping of magnetic fabrics using the anisotropy of magnetic susceptibility of coeval plutons (~500 Ma) at different sectors of the Araçuaí orogen (AO), corresponding to different crustal levels. AO is a large and hot Neoproterozoic orogen situated in the southeast of South America and provides a rare opportunity to study collapsing orogens into their mid to deep crustal sections. The contemporary post-collisional intrusions show structures and magnetic fabrics related to their emplacements, recording different internal flow patterns in the northern and southern portions of the orogen. The contrasting magnetic patterns suggest magma migration from the overthickened orogen core to be stored across its thinner stretched flanks during the gravitational collapse of the orogen edifice. The magma migration across a collapsing large and hot orogens are topics that have been much debated today in high-impact journals. Several studies show predictions of these mechanisms through numerical models. Here, we have a natural case of gravitational collapse in a large and hot orogen that corroborates several numerical models and other cases in nature.

Late-collisional magmatism are products of re-melting process of syn-collisional S-type granites, and are free of the regional solid-state foliation. In the post-collision stage, intrusive plutons were formed, free of regional foliation, and exposed at different crustal levels with a depth range of 10–20 km between the north and the south.

These successive events of magma production imply in high geothermal gradients maintained for a longtime span. Thermobarometric data suggest the middle crust was partially molten (750–920°C) at intermediate to quite high pressures (5–11 kbar) between 600 and 540 Ma in the orogen core (Vauchez et al., 2007). Slow cooling (~3–5°/Myr) persisted up to ~525 Ma, under low decompression (42.5 bar/Ma) and exhumation (157 m/Ma) rates, but it was followed by crustal reheating associated with voluminous production of granitic magma until ~500 Ma (Araujo et al., 2020; Serrano et al., 2018), when the studied plutons were emplaced (Figure 2). The AO merges southward into the NE-trending Ribeira orogen where wrench and strike-slip tectonics dominate in late orogenic stages (Egydio-Silva et al., 2018). The studied plutons are located in the central-eastern Araçuaí orogen and in the Araçuaí–Ribeira boundary sector (Figure 1b).

3 | SAMPLING AND RESULTS

A total of 295 magnetic anisotropy stations were compiled from the literature (references in Figure 2) and 52 new stations

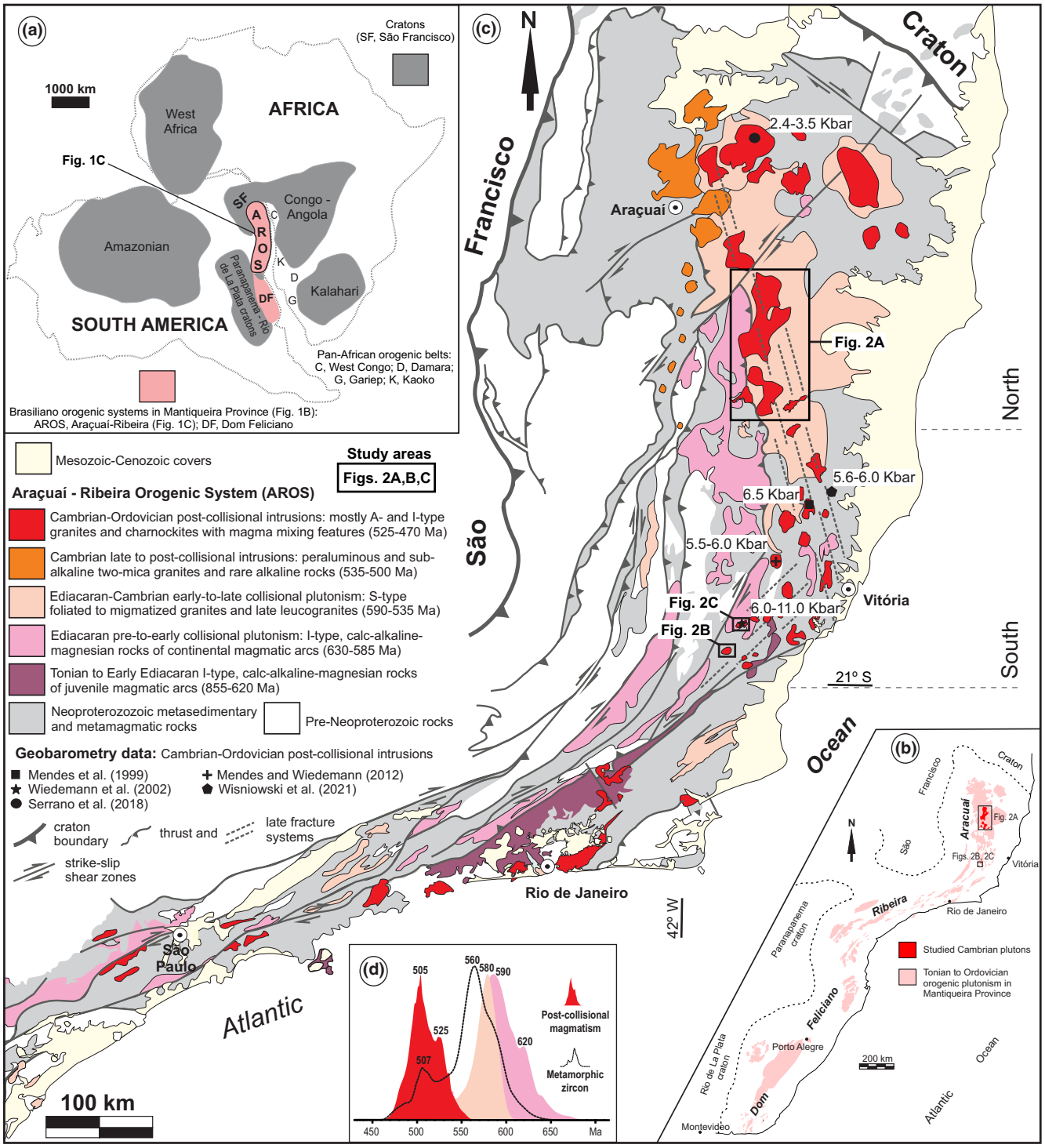

FIGURE 1 (a), the study region in West Gondwana. (b) sketch map highlighting the igneous rocks of the Mantiqueira Province (simplified from Silva et al., 2005). (c) the Araçuaí-Ribeira orogenic system with location of study areas. (d) U–Pb ages for zircons from orogenic igneous rocks, and U–Pb ages for metamorphic zircons (Pedrosa-Soares et al., 2020) and compilation of geobarometry data from post-collisional intrusions. [Colour figure can be viewed at wileyonlinelibrary.com]

were added in the present study. Datasets were compiled for post and syn-collisional granitic rocks from the north (Vargem Grande—VG, and Caladão—C, plutons; Figure 2a) and south domains (Santa Angelica—SA, and Conceição de Muqui—CM plutons; Figure 2b,c). All magnetic measurements were carried out at the Laboratório de Paleomagnetismo of Universidade de São Paulo. In addition, hysteresis loops and measurements of susceptibility against temperature were

performed to characterize the magnetic mineralogy of the rocks (Supplementary Table S2).

Thermomagnetic curves for CM and SA plutons show a simple behaviour during cooling and heating, with steep drops in susceptibility at temperatures of −153°C and 580°C, coincident with the Verwey transition and the Curie temperature of pure magnetite respectively (Supplementary Figure S1). VG and C plutons, in the north, show poorly defined Verwey (−153°C) and Morin (−18°C) transitions that characterize magnetite and haematite respectively (Supplementary Figure S2). Heating of samples from these intrusions causes an increase in susceptibility at ~480°C and a subsequent decrease at ~580°C (Supplementary Figure S2). In all cases, constricted magnetic hysteresis and first-order reversal curves indicate low-coercivity multi-domain magnetite is the main carrier of the magnetic fabric (Supplementary Figure S3; Angelo et al., 2020; Cavalcante et al., 2013; Temporim et al., 2020). This fact is also supported by the values of Mrs/Ms and Hcr/Hc, which are typical of multidomain magnetite (Supplementary Figure S3).

Figure 3 shows AMS parameters for the north and south domains. T x P plot show a dominantly flattened fabric for the northern plutons (red circles), whereas most of those from the south (blue circles) have triaxial ellipsoid shapes with T values ranging from 0.5 to −0.5. The south domain shows high values of Km and P (average 2.999×10^{-3} SI and 1.073 respectively), while the north domain presents low to medium values of Km and P (average 3.809×10^{-2} SI, 1.331 respectively).

Magnetic and field measurements are consistent for both regions. In the north, AMS results are homogenous, with moderate to shallowly dipping magnetic foliation that ranges in strike from NW to NE. Such structural pattern is consistent with magnetic and magmatic foliations reported by Mondou et al. (2012) and Angelo et al. (2020), as well as with the double-verging ductile fabrics of the central orogen core (Novo et al., 2018). The C pluton shows shallowly dipping NS to NE-striking magnetic foliations with a magnetic lineation that plunges gently to the SW. Magnetic foliations within the VG pluton (Figure 2a) dip gently to the NE to NW with a sub-horizontal NNW-trending magnetic lineation. A small subset of samples from the VG pluton has subvertical magnetic lineations (Figure 2a). In contrast, the south domain rocks are defined by concentric patterns of lithology distribution and structural fabric (Figures 2b,c), with gently dipping NE to E-trending lineations at felsic borders and vertical in the mafic cores (Figure 2c).

Microstructural analysis throughout the post-collisional plutons from northern and southern portion of the AO confirms the predominance of magmatic deformation features. Most of the magmatic state is supported by the well-oriented magmatic fabric (Supplementary Figure S4). Detailed description is found in the Supplementary.

4 | DISCUSSION

Post-collisional plutons (~500 Ma) show distinct relations to the regional structural framework. In the north (Figure 2a), early-to-late collisional granites and amphibolite-facies migmatites (785°C and 7.5 kbar, Richter et al., 2016) are the main host rocks enclosing post-collisional plutons. In the south (Figure 2b), plutons are hosted by high-amphibolite to granulite facies rocks (670–860°C and 5.24–10.2 kbar, Gouvêa et al., 2020) of the Ediacaran magmatic arc and related supracrustal rocks. Before magmatic quiescence between 545 and 525 Ma in the north domain, high amounts of melt hindered strain localization into major strike-slip shear zones (Melo et al., 2017). Both areas attained the metamorphic peak at ~560 Ma (Araujo et al., 2020; Pedrosa-Soares et al., 2020). Under such conditions, strain is widely distributed in the middle crust, taken up wherever melt is present (Vauchez et al., 2007). The syn-collisional granitic rocks show a variably oriented magnetic pattern but mostly shallowly dipping, with a lineation varying from perpendicular (E-W) to locally parallel (N-S) to the orogen. The north domain post-collisional plutons show a low-angle NW to NE trending magnetic foliation bearing a down-dip magnetic lineation following the general trend of the orogen (Figure 2a). However, the low-angle NW to NE-striking magnetic pattern is consistent with the regional magnetic pattern and tectonic framework of the AROS central orogen core, suggesting magma migration along the main NS-trending structures and final emplacement. In the south, the fabric developed during the late collisional event is concentrated along previous dextral strike-slip shear zones. The SA and CM plutons are located distal to the hot interior where some post-collisional plutons were emplaced along high-angle, ductile shear zones and in the core of pre-existing antiformal structures (De Campos et al., 2016). They are nearly isotropic in the field, and truncate previously developed fabrics.

During orogen collapse the outward gravitational spreading drives thrusting at the flanks of the orogen that is simultaneous with ductile extension and thinning in the core (Rey et al., 2001). The flow direction follows the path of least resistance. Usually, 2D models are incapable of modelling the complexity of the orogen-parallel post-convergent processes. But orogen-parallel mass flow is ubiquitous in active and past orogens reported in the Tibetan Plateau (Royden et al., 2008), the Eastern Alps (Frisch et al., 2000) and the Canadian Cordillera (Vanderhaeghe & Teyssier, 2001a). The current AROS crustal exposures allow us to depict the different regimes of post-collisional magmatic ascent and migration along-strike and across a crustal section comprising the shallow crust in the north and deeper crustal levels in the south.

Figure 4 represents a crustal block diagram during orogen collapse. In the north, upper crust thinning was accommodated by E-W extension recorded in low-angle shear zones that operated

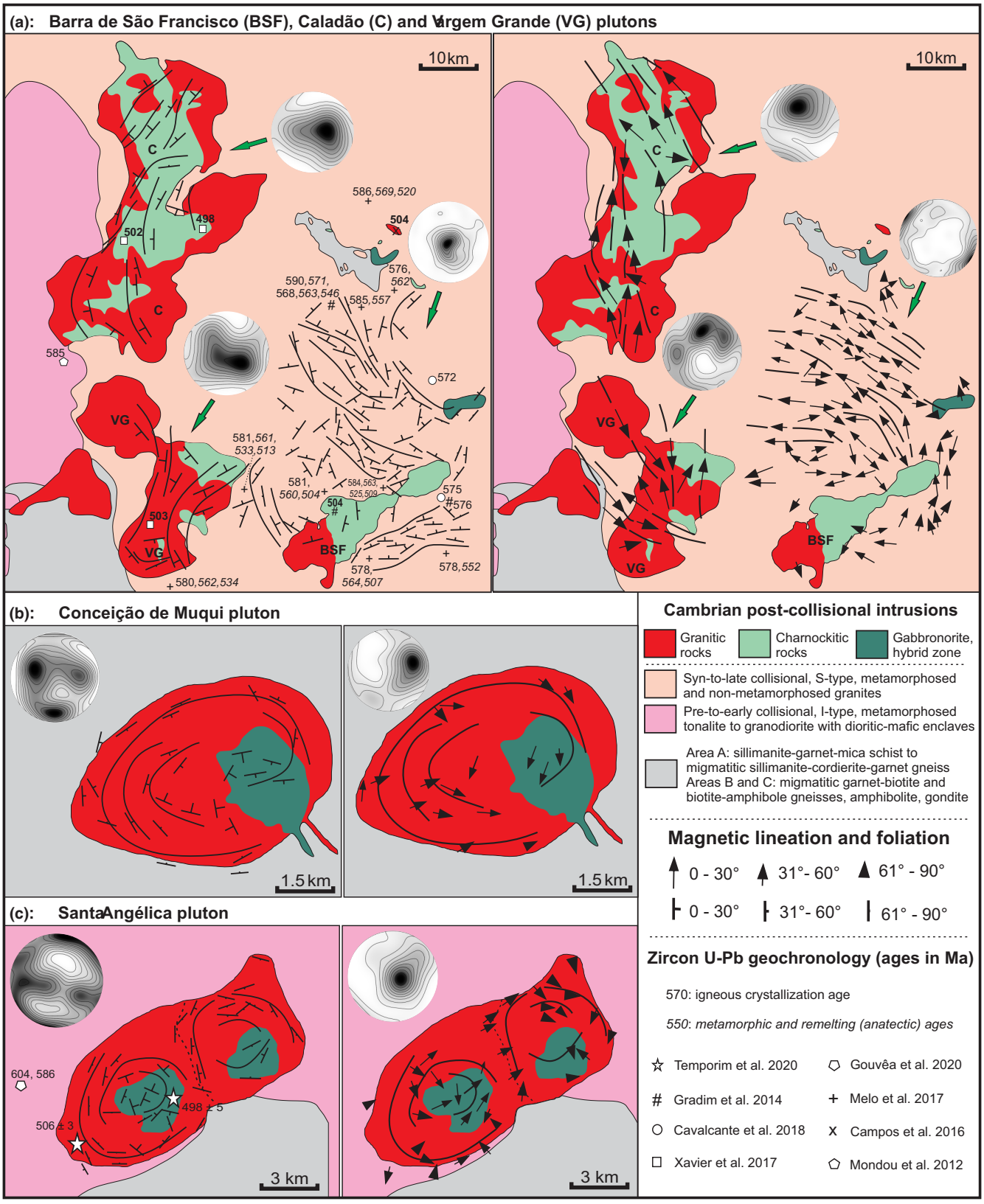

FIGURE 2 Magnetic fabric of post-collisional plutons and compilation of U–Pb radiometric ages for the north (a) and south (b and c) study areas. Stereoplots for AMS fabric are displayed for each studied pluton. Magnetic data sources: Vargem Grande, this study; Xavier (2017); Angelo et al. (2020); Barra do São Francisco, Cavalcante et al. (2013); Caladão, this study, Mondou et al. (2012); Xavier (2017); Angelo et al. (2020); Conceição de Muqui: This study; Santa Angélica: Temporim et al. (2020). [Colour figure can be viewed at wileyonlinelibrary.com]

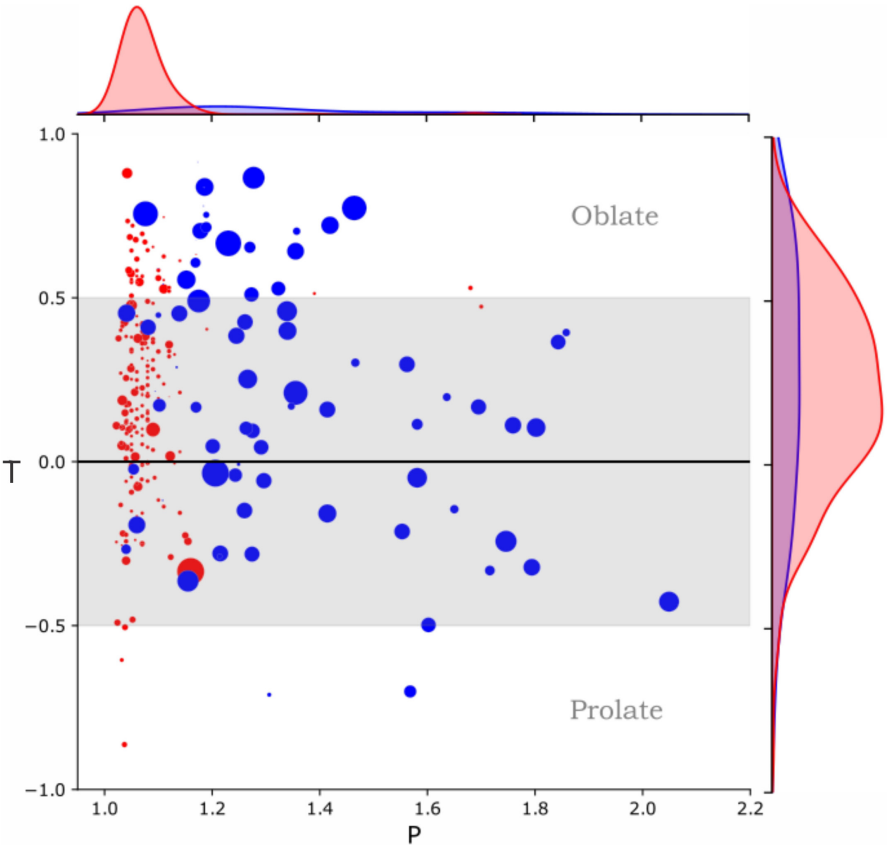

FIGURE 3 Jelinek plot (TxP). Red and blue circles represent north and south domain, respectively, and the size of the circles varies with the bulk magnetic susceptibility (km). The dispersion of the T and P parameters also is shown in the figure. [Colour figure can be viewed at wileyonlinelibrary.com]

synchronously to the extensive post-tectonic granite plutonism (Peixoto et al., 2017), showing that the whole crust was involved in orogen collapse. Recently, Santiago et al. (2020) identified the last episode of mantle-derived magmatism in the AO, represented by mafic dike swarms associated with the collapsing orogen (500 Ma).

Inside the orogenic core, the dominant structures are subhorizontal foliations associated with flattening and horizontal along-strike mass flow (Figures 2a and 4). Previously formed steeply dipping structures may have been strongly obliterated by this mass flow. In the south, deeper in the crust, the feeding zones of this large post-collisional magmatism are represented by vertical fabrics (Figures 3 and 4) in the plutons with a strong contribution of mantle-derived magmas, sometimes mingled with the granitic types or forming the nuclei of the intrusions.

Such specific relationships between the steep orogenic structures at the orogenic flanks and the late, pervasive subhorizontal structures in the orogenic core, are also observed in other large and hot orogens (e.g. Grenville orogen, Jamieson et al., 2010). An orogenic plateau have developed during the Ottawan orogeny, based on widespread fabrics indicating flattening and subhorizontal flow at synorogenic event (Culshaw et al., 1997). When tectonic convergence ends, the orogens undergo gravitational spreading, in which middle and lower crust flow laterally from the plateau towards the flanks, driving thrusting on the orogenic flanks and ductile thinning in the orogenic core. The flow direction will be determined by the path of least resistance, commonly by shear zones cutting the crust, which may change as the system evolves. In the case of 2-D post-orogenic gravitational spreading, ductile thinning in the core drives thrusting in the orogenic foreland (e.g. Rey et al., 2001). Model feasibility is tested against data from the western Grenville Orogen in Ontario by Jamieson and Beaumont (2011). Although exhumation at the flanks is dominated by the effects of syn-convergent thrusting and erosion, post-convergent ductile thinning in the orogenic core leads to exhumation of a broad region of lower crust by about 10–30 km.

Since in the AROS these different lithotectonic domains were exhumed, we have a rare opportunity to actually see this rheological stratification (Figure 4) and the root from where large volumes of magma originated from the mantle and the mantle–crust boundary (De Campos et al., 2016). These magmas were likely entrained by the relatively steep shear zones that transect the metamorphic sequence and border the plutons in the southern sector, cutting down into the deep crust as predicted in numerical models (Jamieson & Beaumont, 2011). In this case, the emplacement of hot material over a cooler substrate is commonly interpreted as resulting in an "inverted" metamorphic sequence (Jamieson & Beaumont, 2013), with a peak temperature at the partially molten mid-crustal section (Figure 4).

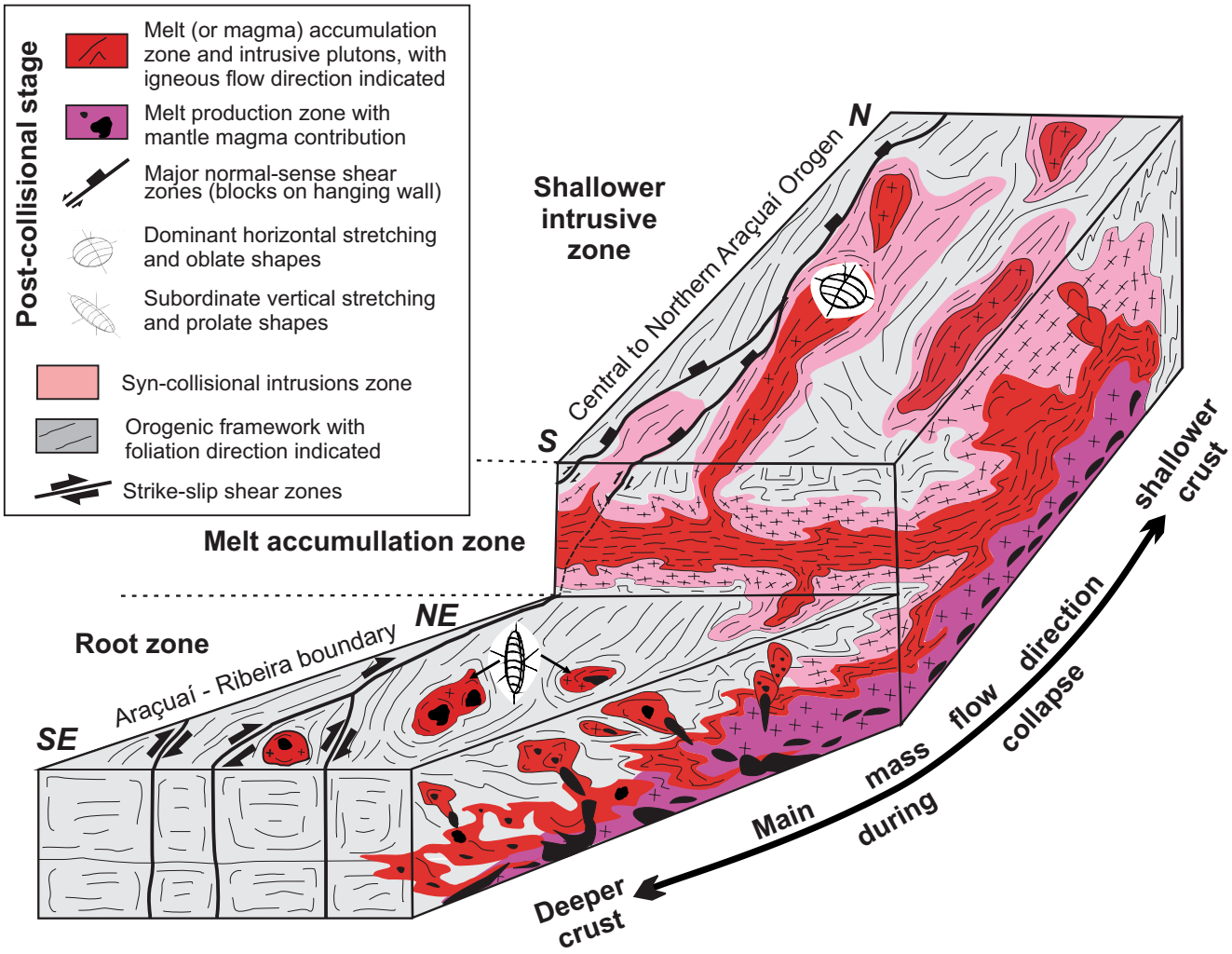

FIGURE 4 Schematic 3D cross-section of orogen-parallel post-convergent gravitational collapse at ~500 ma. A substantial amount of orogenic core material in the form of hybrid magma was transported through NE-trending shear zones and emplaced at the mid-crust. [Colour figure can be viewed at wileyonlinelibrary.com]

5 | CONCLUSION

In the collapse phase, contrasting rheological behaviour of the crust at different levels is well marked by the structures in magmatic rocks from northern to southern Araçuai-Ribeira orogenic system. In the north, post-collisional magmatic rocks have ~NS-trending magnetic foliations following the collisional tectonic framework and marking a general along-strike magmatic flow from south to north, that is, from deeper to shallower crustal levels. In turn, coeval deep-seated intrusions in the south present a concentric distribution of foliations and lineations, in striking contrast with the general NE–SW trend of the host rocks. Such contrasting magnetic patterns coupled with structural fabrics and geochemical signatures demonstrate that gravitational collapse was accompanied by the generation of abundant magmatism in the orogen's hot keel that flowed from these deep sources to its previously stretched flanks.

ACKNOWLEDGEMENTS

Funds were granted by São Paulo Research Foundation (#2016/06114-6 and #2017/11672-0); Coordenação de Aperfeiçoamento de Pessoal de Nível Superior, Brasil (CAPES/SIU 0013) and Conselho Nacional de Desenvolvimento Científico e Tecnológico (#405954/2016-6 and #304214/2018-3).

DATA AVAILABILITY STATEMENT

The data that support the findings of this study are available from the corresponding author upon reasonable request.

REFERENCES

Alkmim, S., Marshak, A. C., Pedrosa-Soares, G. G., Peres, S. C. P., & Cruz, A. W. (2006). Kinematic evolution of the Araçuaí-West Congo orogen in Brazil and Africa: Nutcracker tectonics during the Neoproterozoic assembly of Gondwana. *Precambrian Research*, *149*, 43–64.

Angelo, T. V., Egydio-Silva, M., Temporim, F. A., & Seraine, M. (2020). Midcrust deformation regime variations across the Neoproterozoic

Araçuaí hot orogen (SE Brazil): Insights from structural and magnetic fabric analyses. *Journal of Structural Geology*, *134*, 104007. https://doi.org/10.1016/j.jsg.2020.104007

Araujo, C., Pedrosa-Soares, A., Lana, C., Dussin, I., Queiroga, G., Serrano, P., & Medeiros-Junior, E. (2020). Zircon in emplacement borders of post-collisional plutons compared to country rocks: A study on morphology, internal texture, U-Th-Pb geochronology and Hf isotopes (Araçuaí orogen, SE Brazil). *Lithos*, *352*, 105252. https://doi.org/10.1016/j.lithos.2019.105252

Cavalcante, C., Hollanda, M. H., Vauchez, A., & Kawata, M. (2018). How long can the middle crust remain partially molten during orogeny? *Geology*, *46*, 839–842. https://doi.org/10.1130/G45126.1

Cavalcante, G. C. G., Egydio-Silva, M., Vauchez, A., & Camps, P. (2013). Strain distribution across a partially molten middle crust: Insights from the AMS mapping of the Carlos Chagas Anatexite, Araçuaí belt (East Brazil). *Journal of Structural Geology*, *55*, 79–100. https://doi.org/10.1016/j.jsg.2013.08.001

Caxito, F., Hartmann, L., Heilbron, M., Pedrosa-Soares, A., Bruno, H., Basei, M., & Chemale, F. (2022). Multi-proxy evidence for subduction of the Neoproterozoic Adamastor Ocean and Wilson cycle tectonics in the South Atlantic Brasiliano Orogenic System of western Gondwana. Precambrian Research, 376, 106678.

Culshaw, N. G., Jamieson, R. A., Ketchum, J. W. F., Wodicka, N., Corrigan, D., & Reynolds, P. H. (1997). Transect across the northwestern Grenville Orogen, Georgian bay, Ontario: Polystage convergence and extension in the lower orogenic crust. *Tectonics*, *16*, 966–982. https://doi.org/10.1029/97TC02285

De Campos, C. M., Medeiros, S. R., Mendes, J. C., Pedrosa-Soares, A. C., Dussin, I., Ludka, I. P., & Dantas, E. L. (2016). Cambro-Ordovician magmatism in the Araçuaí Belt (SE Brazil): Snapshots from a post-collisional event. *Journal of South American Earth Sciences*, *68*, 248–268. https://doi.org/10.1016/j.jsames.2015.11.016

Egydio-Silva, M., Vauchez, A., Fossen, H., Cavalcante, C. G., & Xavier, B. C. (2018). Connecting the Araçuaí and Ribeira belts (SE–Brazil): Progressive transition from contractional to transpressive strain regime during the Brasiliano orogeny. *Journal of South American Earth Sciences*, *86*, 127–139. https://doi.org/10.1016/j.jsames.2018.06.005

Frisch, W., Dunkl, I., & Kuhlemann, J. (2000). Post-collisional orogen-parallel large-scale extension in the eastern Alps. *Tectonophysics*, *327*, 239–265. https://doi.org/10.1016/S0040-1951(00)00204-3

Gouvêa, L. P., Medeiros, S. R., Mendes, J. C., Soares, C., Marques, R., & Melo, M. (2020). Magmatic activity period and estimation of P-T metamorphic conditions of pre-collisional opx-metatonalite from Araçuaí-Ribeira orogens boundary, SE Brazil. *Journal of South American Earth Sciences*, *99*, 102506. https://doi.org/10.1016/j.jsames.2020.102506

Henk, A., von Blanckenburg, F., Finger, F., Schaltegger, U., & Zulauf, G. (2000). Syn-convergent high-temperature metamorphism and magmatism in the Variscides: A discussion of potential heat sources. *Geological Society, London, Special Publications*, *179*, 387–399. https://doi.org/10.1144/GSL.SP.2000.179.01.23

Jamieson, R. A., & Beaumont, C. (2011). Coeval thrusting and extension during post-convergent ductile flow - implications for exhumation of high-grade metamorphic rocks. *Journal of Metamorphic Geology*, *29*, 33–51. https://doi.org/10.1111/j.1525-1314.2010.00908.x

Jamieson, R. A., & Beaumont, C. (2013). On the origin of orogens. *GSA Bulletin*, *125*, 1671–1702. https://doi.org/10.1130/B30855.1

Jamieson, R. A., Beaumont, D., Warren, C. J., & Nguyen, M. H. (2010). The Grenville Orogen explained? Applications and limitations of integrating numerical models with geological and geophysical data. *Canadian Journal of Earth Sciences*, *47*, 517–539.

Melo, M. G., Lana, C., Stevens, G., Pedrosa-Soares, A. C., Gerdes, A., Alkmin, L. A., Nalini, H. A., Jr., & Alkmim, F. F. (2017). Assessing the isotopic evolution of S-type granites of the Carlos Chagas batholith, SE Brazil: Clues from U-Pb, Hf isotopes, Ti geothermometry and trace element composition of zircon. *Lithos*, *284*, 730–750.

Mondou, M., Egydio-Silva, M., Vauchez, A., Raposo, M. I. B., Bruguier, O., & Oliveira, A. F. (2012). Complex, 3D strain patterns in a synkinematic tonalite batholith from the Araçuaí Neoproterozoic orogen (eastern Brazil): Evidence from combined magnetic and isotopic chronology studies. *Journal of Structural Geology*, *39*, 158–179. https://doi.org/10.1016/j.jsg.2012.02.015

Novo, T. A., Pedrosa-Soares, A., Vieira, V. S., Dussin, I., & Silva, L. C. (2018). The Rio Doce group revisited: An Ediacaran arc-related volcano-sedimentary basin, Araçuaí orogen (SE Brazil). *Journal of South American Earth Sciences*, *85*, 345–361.

Pedrosa-Soares, A. C., Deluca, C., Araujo, C. S., Gradim, C., Lana, C., Dussin, I., Silva, L. C., & Babinski, M. (2020). O Orógeno Araçuaí à luz da geocronologia: um tributo a Umberto Cordani. In *Geocronologia e evolução tectônica do Continente Sul-Americano: A contribuição de Umberto Giuseppe Cordani* (pp. 250–272). Solaris Edições Culturais.

Peixoto, E., Alkmim, F. F., Pedrosa-Soares, A., Lana, C., & Chaves, A. O. (2017). Metamorphic record of collision and collapse in the Ediacaran-Cambrian Araçuaí orogen, SE-Brazil: Insights from P–T pseudosections and monazite dating. *Journal of Metamorphic Geology*, *36*, 147–172. https://doi.org/10.1111/jmg.12287

Rey, P., Vanderhaeghe, O., & Teyssier, C. (2001). Gravitational collapse of the continental crust: Definition, regimes and modes. *Tectonophysics*, *342*, 435–449. https://doi.org/10.1016/S0040-1951(01)00174-3

Richter, F., Lana, C., Stevens, G., Buick, I., Pedrosa-Soares, A. C., Alkmim, F. F., & Cuttsa, K. (2016). Sedimentation, metamorphism and granite generation in a back-arcregion: Records from the Ediacaran Nova Venécia Complex (Arac¸uaíOrogen, Southeastern Brazil). *Precambrian Research*, *272*, 78–100. https://doi.org/10.1016/j.precamres.2015.10.012.

Royden, L. H., Burchfiel, B. C., & van der Hilst, R. V. (2008). The geological evolution of the Tibetan plateau. *Science*, *321*, 1054–1058. https://doi.org/10.1126/science.1155371

Santiago, R., Caxito, F. A., Neves, M. A., Dantas, E. L., Medeiros Junior, E. B., & Queiroga, G. N. (2020). Two generations of mafic dyke swarms in the southeastern Brazilian coast: Reactivation of structural lineaments during the gravitational collapse of the Araçuaí-Ribeira Orogen (500 ma) and West Gondwana breakup (140 ma). *Precambrian Research*, *340*, 105344. https://doi.org/10.1016/j.precamres.2019.105344

Serrano, P., Pedrosa-Soares, A., Medeiros-Junior, E., Fonte-Boa, T., Araujo, C., Dussin, I., Queiroga, G., & Lana, G. (2018). A-type Medina batholith and post-collisional anatexis in the Araçuaí orogen (SE Brazil). *Lithos*, *320*, 515–536. https://doi.org/10.1016/j.lithos.2018.09.009

Silva, L. C. d., McNaughton, N. J., Armstrong, R., Hartmann, L. A., & Fletcher, I. R. (2005). The Neoproterozoic Mantiqueira Province and its African connections: a zircon-based U–Pb geochronologic subdivision for the Brasiliano/Pan-African systems of orogens. *Precambrian Research*, *136*, 203–240.

Temporim, F. A., Trindade, R. I. F., Tohver, E., Soares, C. C., Gouvêa, L. P., Egydio-Silva, M., Amaral, C. A. D., & Souza, G. F., Jr. (2020). Magnetic fabric and geochronology of a Cambrian "isotropic" pluton in the Neoproterozoic Araçuaí orogeny. *Tectonics*, *39*, e2019TC005877. https://doi.org/10.1029/2019TC005877

Vanderhaeghe, O., & Teyssier, C. (2001a). Crustal-scale rheological transitions during late-orogenic collapse. *Tectonophysics*, *335*, 211–228. https://doi.org/10.1016/S0040-1951(01)00053-1

Vanderhaeghe, O., & Teyssier, C. (2001b). Partial melting and flow of orogens. *Tectonophysics*, *342*, 451–472.

Vauchez, A., Egydio-Silva, M., Babinski, M., Tommasi, A., Uhlein, A., & Liu, D. (2007). Deformation of a pervasively molten middle crust: Insights from the Neoproterozoic Ribeira-Araçuaí orogen (SE Brazil). *Terra Nova*, *19*, 278–286. https://doi.org/10.1111/j.1365-3121.2007.00747.x

Xavier, B. C., 2017. Relações tectônicas no Central da Faixa Araçuaí: Análise estrutural por AMS e geocronologia U/Pb e Lu/Rf. Unpubl. Msc Thesis, Universidade de São Paulo, 123 pp.

SUPPORTING INFORMATION

Additional supporting information can be found online in the Supporting Information section at the end of this article.

FIGURE S1 Representative thermomagnetic curves for four samples of Conceição de Muqui pluton. The y-axis is the bulk of magnetic susceptibility and the x-axis is the temperature in degrees Celsius. The red lines represent the heating and blue lines represent the cooling.

FIGURE S2 Representative thermomagnetic curves for two samples of both Padre Paraíso charnockite and Caladão granite. The y-axis is the bulk of magnetic susceptibility and the x-axis is the temperature in degrees Celsius. The red lines represent the heating and blue lines represent the cooling.

FIGURE S3 Hysteresis loops for six samples which represents all the lithotypes present measured in this work. Mrs/Ms and Hcr/Hc rates (Day et al., 1977).

FIGURE S4 Photomicrographs of microstructures of the Santa Angélica Pluton: (a) undulose extinction in quartz. Conceição de Muqui pluton: (b) deformed twins in plagioclase, (c) microfractures and embayments in deformed feldspars filled by a fine-grained mosaic of quartz and/or plagioclase. Caladão pluton: (d) interstitial quartz grains with irregular and curved boundaries, (e) local solid-state features with a chessboard-like pattern in quartz and magmatic features with deformation twins in plagioclase. Santa Angélica microstructures - Temporim et al. (2020) and Caladão microstructures - Angelo et al. (2020).

TABLE S1 Main characteristics of the G1 to G5 supersuites of the Araçuaí orogen (after Pedrosa-Soares et al., 2011, 2020, Serrano et al., 2018, and Wisniowscky et al., 2021, updated with data from Gouvêa et al., 2020; Soares et al., 2020; Temporim et al., 2020; and the present paper).

TABLE S2 Anisotropy of magnetic susceptibility parameters of the Caladão granite, Padre Paraíso charnockite, Conceição de Muqui pluton and Santa Angélica pluton. Site number; location (UTM) in meters; Km = mean magnetic susceptibility (10^{-4} SI); P = degree of anisotropy of the magnetic susceptibility ($P = k_1/k_3$);T = AMS ellipsoid shape parameter [$T = 2\ln(k_2/k_3)/\ln(k_1/k_3) - 1$]; K_1 = trend and plunge of magnetic lineation (in degrees); K_2 = trend and plunge of the intermediate anisotropy axis; K_3 = trend and plunge of the pole of the magnetic foliation; ε_{12}, ε_{23}, ε_{31} are the semi-angle (measured in degrees) of confidence ellipses of AMS axes from Jelínek's (1978) statistics. AR, CM - this work; [1]AR - Mondou et al. (2012); [2]AR - Cavalcante et al. (2013); MBS - Xavier et al. (2017); TM - Angelo et al. (2019); SA - Temporim et al. (2020).

How to cite this article: Temporim, F. A., da Trindade, R. I. F., Egydio-Silva, M., Angelo, T. V., Tohver, E., Soares, C. C., Gouvêa, L. P., Mendes, J. C., Medeiros, S. R., Pedrosa-Soares, A. C., & Silva, G. G. (2023). Vertical deformation partitioning across a collapsing large and hot orogen. *Terra Nova*, *35*, 23–31. https://doi.org/10.1111/ter.12625